

Learning Multi-Modal Mobility Dynamics for Generalized Next Location Recommendation

Junshu Dai
Zhejiang University
Hangzhou, Zhejiang, China
djs@zju.edu.cn

Wei Ji
Nanjing University
Nanjing, Jiangsu, China
weiji0523@gmail.com

Jie Song
Zhejiang University
Hangzhou, Zhejiang, China
sjie@zju.edu.cn

Yu Wang
Zhejiang University
Hangzhou, Zhejiang, China
yu.wang@zju.edu.cn

Qinghong Guo
Zhejiang University
Hangzhou, Zhejiang, China
q.h_guo@zju.edu.cn

Canghong Jin
Hangzhou City University
Hangzhou, Zhejiang, China
jinch@zucc.edu.cn

Tongya Zheng*
Hangzhou City University
Hangzhou, Zhejiang, China
doujiang_zheng@163.com

Ji Cao
Zhejiang University
Hangzhou, Zhejiang, China
caoj25@zju.edu.cn

Mingli Song
Zhejiang University
Hangzhou, Zhejiang, China
brooksong@zju.edu.cn

Abstract

The precise prediction of human mobility has produced significant socioeconomic impacts, such as location recommendations and evacuation suggestions. However, existing methods suffer from limited generalization capability: unimodal approaches are constrained by data sparsity and inherent biases, while multi-modal methods struggle to effectively capture mobility dynamics caused by the semantic gap between static multi-modal representation and spatial-temporal dynamics. Therefore, we leverage multi-modal spatial-temporal knowledge to characterize mobility dynamics for the location recommendation task, dubbed as **Multi-Modal Mobility (M^3 ob)**. First, we construct a unified spatial-temporal relational graph (STRG) for multi-modal representation, by leveraging the functional semantics and spatial-temporal knowledge captured by the large language models (LLMs)-enhanced spatial-temporal knowledge graph (STKG). Second, we design a gating mechanism to fuse spatial-temporal graph representations of different modalities, and propose an STKG-guided cross-modal alignment to inject spatial-temporal dynamic knowledge into the static image modality. Extensive experiments on six public datasets show that our proposed method not only achieves consistent improvements in normal scenarios but also exhibits significant generalization ability in abnormal scenarios. Our code will be made publicly available at <https://anonymous.4open.science/r/M3ob-62EF>.

CCS Concepts

• Information systems → Recommender systems.

*Corresponding author.

Permission to make digital or hard copies of all or part of this work for personal or classroom use is granted without fee provided that copies are not made or distributed for profit or commercial advantage and that copies bear this notice and the full citation on the first page. Copyrights for components of this work owned by others than the author(s) must be honored. Abstracting with credit is permitted. To copy otherwise, or republish, to post on servers or to redistribute to lists, requires prior specific permission and/or a fee. Request permissions from permissions@acm.org.

Conference acronym 'XX, Woodstock, NY

© 2018 Copyright held by the owner/author(s). Publication rights licensed to ACM.

ACM ISBN 978-1-4503-XXXX-X/2018/06

<https://doi.org/XXXXXXX.XXXXXXX>

Keywords

Recommender systems, POI recommendation, Multi-modal

ACM Reference Format:

Junshu Dai, Yu Wang, Tongya Zheng, Wei Ji, Qinghong Guo, Ji Cao, Jie Song, Canghong Jin, and Mingli Song. 2018. Learning Multi-Modal Mobility Dynamics for Generalized Next Location Recommendation. In *Proceedings of Make sure to enter the correct conference title from your rights confirmation email (Conference acronym 'XX)*. ACM, New York, NY, USA, 13 pages. <https://doi.org/XXXXXXX.XXXXXXX>

1 Introduction

The widely adopted mobile devices have made location-based services highly accessible on the Web, allowing applications such as location search [14, 42], mobile navigation [37], and location recommendation [21, 45]. However, while the related check-in sequence data greatly facilitates the integration of web services into daily life, two issues lead to data sparsity: the sheer number of locations, and users' tendency to visit only a limited number of popular locations of interest. Furthermore, abnormal mobility behaviors are difficult to capture due to their scarce occurrence, such as visits to long-tail locations or during extreme weather events.

The remarkable success of deep learning has transformed next location recommendation into a representation learning paradigm, which can be categorized into sequence-based methods and graph-based methods. Sequence-based methods design spatial-temporal modules to extract mobility representations within historical check-in sequences, including markov chain-based model [8], RNNs-based model [28, 41] and attention-based model [6, 7, 23, 30]. Graph-based methods [3, 9, 15, 24–27, 34, 40, 43] enhance location representations by sharing common patterns of locations based on spatial-temporal graphs. However, the sparsity of check-in sequences and the inherent mobility bias lead to suboptimal performance in representation learning for these unimodal approaches.

Recently, language and vision models have demonstrated advanced representations based on sufficient self-supervised learning, which inspires the progress of multi-modal learning across various domains. In e-commerce recommendation, MKGAT [29] and

MMGCN [36] leverage multi-modal attributes of items together with abundant user-item interactions to construct a multi-modal graph for learning. Alignrec [22] narrows the representation distance through contrastive learning between items and their multi-modal content. In location recommendation, to our knowledge, MMPOI [39] was the first to introduce multi-modality by constructing a multi-modal graph via cosine similarity. However, existing multi-modal approaches neglect the semantic gap between mobility dynamics and static multi-modal representations, thus inevitably leading to performance degradation when generalizing.

Despite the effectiveness of multi-modal pre-training representations, bridging the semantic heterogeneity between static multi-modal data and dynamic human mobility remains a key challenge.

(1) How to model the dynamic relationships of locations and users in a multi-modal view? Current multi-modal methods construct static multi-modal relationships to obtain multi-modal knowledge without integrated mobility dynamics, leading to limited generalization capability in dynamic scenarios. **(2) How to align multi-modal representations of locations and users to capture mobility dynamics?** The inherent semantic gap between different modalities necessitates spatial-temporal-aware alignment techniques to eliminate the modality heterogeneity.

To this end, we design a **Multi-Modal Mobility ($M^3\text{ob}$)** framework that overcomes the generalization gap by building a shared graph across multiple modalities.

To address the first challenge of modeling multi-modal dynamics, we build a spatial-temporal relational graph (STRG) to enable the sharing of spatial-temporal knowledge across modalities, which leverages the functional semantics and spatial-temporal knowledge from a large language models (LLMs)-enhanced spatial-temporal knowledge graph (STKG). The hierarchical knowledge from the STKG further enables the modeling of multi-level user preferences. For the second challenge of aligning multi-modal representations, we employ a gating mechanism to dynamically fuse spatial-temporal graph representations from different modalities, thereby mitigating modal interference. Additionally, STKG-guided cross-modal alignment is applied to reduce inter-modal discrepancies.

Our main contributions are summarized as follows:

- We propose **$M^3\text{ob}$** , a novel framework for seamlessly fusing and aligning dynamic human mobility patterns with static multi-modal representations.
- We construct a new STRG based on LLMs-enhanced STKG to unify multi-modal mobility representations and leverage STKG-guided cross-modal alignment to improve the spatial-temporal dynamics of static image modality.
- Experimental results show that **$M^3\text{ob}$** achieves a superior performance gain over the baseline, with robust generalization in adverse weather and long-tail scenarios, and high efficiency.

2 Related Work

2.1 Next Location Recommendation

Deep learning approaches have dominated the advanced progress of next location recommendation, which predicts users' future visits and can be categorized into sequence-based and graph-based models. **Sequence-based models** capture spatial-temporal patterns through Markov chains [8], RNN architectures [7, 28, 41, 46],

Table 1: Comparison between our $M^3\text{ob}$ against baseline methods. STKG denotes Spatial-Temporal Knowledge Graph.

Methods	Location		User
	Multi-modal Graph	Alignment	Preference
GETNEXT [43]	✗	✗	Single-level
DisenPOI [24]	✗	Data-based	Single-level
Diff-POI [25]	✗	✗	Single-level
STHGCN [40]	✗	✗	Single-level
CLSPRec [6]	✗	Data-based	Single-level
AGCL [27]	✗	Graph-based	Single-level
MCLP [30]	✗	✗	Single-level
LoTNext [38]	✗	✗	Single-level
MMPOI [39]	Cosine Similarity	✗	Single-level
TSPN-RA [12]	Quad Tree	✗	Single-level
$M^3\text{ob}$ (Ours)	STKG-based	STKG-based	Multi-level

or attention mechanisms [23, 30]. For instance, LSTPM [28] employs a non-local network and a geographically dilated RNN to model long- and short-term preferences. CLSPRec [6] leverages contrastive learning on raw sequential data to effectively distinguish between long- and short-term user preferences. MCLP [30] incorporates a multi-head attention mechanism to generate arrival time embeddings as contextual information for location recommendation. However, these methods insufficiently capture the spatial-temporal transition patterns of different locations in trajectories. **Graph-based models** primarily utilize spatial-temporal relationships between locations and apply GNNs to enhance location representations. A line of works enhance location embeddings by constructing spatial-temporal graphs based on geographical and transitional relationships between locations [9, 15, 25, 43]. GETNEXT [43] constructs a global trajectory flow graph to better capture transition patterns between locations. Another line of works builds spatial-temporal mobility graphs using pre-trained spatial-temporal knowledge graphs [26, 38, 44]. AGCL [27] employs graph-enhanced location representation and negative-sample contrast to enhance the discriminability and consistency of POI representations. LoTNext [38] introduces long-tailed adjustment strategies for both graph and loss to tackle the imbalance between head and tail locations. However, unimodal check-in sequences inevitably limit the representation quality of these methods, yielding suboptimal generalization capability in scarce mobility scenarios. Recent studies have attempted to alleviate this sparsity issue by enriching the semantic features of locations with multi-modal information. MMPOI [39] constructs static multi-modal graphs using intra-modal cosine similarity to leverage independent information from each modality. TSPN-RA [12] builds a spatial graph based on a static quadtree structure derived from remote sensing imagery to incorporate real-world environmental semantics. However, static relationships of locations extracted from multi-modal mobility data overlook the spatial-temporal dynamics, thereby leaving significant semantic gaps between multi-modal embedding and mobility learning. Table 1 illustrates that we inject mobility dynamics into multi-modal representation beyond limitations of existing methods.

2.2 Multi-Modal Recommendation

Multi-modal content, which enriches item information and captures users' fine-grained preferences, has been widely introduced into recommendation systems in recent studies [19, 47]. Existing research has effectively integrated multi-modal information through the integration of attention mechanisms [4, 16, 18, 20]. Another line of work constructs multi-modal graphs based on user-item interactions and item multi-modal attributes to enrich item semantic representations [31, 32, 35, 36]. Further advancing this direction, several studies leverage multi-modal knowledge graphs to model complex interactions between users and multi-modal information [17, 29, 33]. Another approach [22, 48] seeks alignment in the representation space, diminishing the distance between representations through the adoption of contrastive learning between items and their multi-modal content. Existing multi-modal recommendation primarily focuses on static modal fusion and fails to model the inherent spatiotemporal dynamics of mobile data, making it difficult to be directly applied to mobility representation tasks.

3 Preliminary

Trajectory Sequence. The set of locations is denoted as $P = \{p_1, p_2, \dots, p_{N_p}\}$ and the set of users is $U = \{u_1, u_2, \dots, u_{N_u}\}$, where N_p and N_u are the total number of locations and users respectively. Each record is denoted by a tuple $q = \{u, p, t\}$, indicating that user u visited location p at time t . The trajectory of each user $u \in U$ is denoted by $S_u = \{q_u^1, q_u^2, \dots\}$.

Multi-modal Location. A location p can be represented in either an ID modality or a pair of latitude and longitude. In this paper, we augment the location semantics by textual and visual modalities. Moreover, the textual modality of a location is extended to hierarchical semantics, from the location category c to the user activity a , denoted by $p_{\text{text}} = \{p, c, a\}$. On the other hand, the visual modality of a location is denoted by remote sensing images at different zoom levels, denoted by $p_{\text{img}} = \{p_{\text{img}}^h \mid h \in \mathcal{H}\}$, where $\mathcal{H} = \{\text{coarse, medium, fine}\}$.

Next Location Recommendation. Given a user's trajectory sequence $\{q_u^1, q_u^2, \dots, q_u^n\}$, our goal is to predict the next location p_{n+1} that user u most likely to visit.

4 Methodology

Figure 1 demonstrates that the overall workflow of our proposed **M³ob** framework can be divided into three parts. (a) Spatial-Temporal Knowledge Graph (STKG) enriches the spatial-temporal semantics by LLM-enhanced textual semantics of spatial-temporal entities. (b) Leveraging the unified embedding space of the Spatial-Temporal Knowledge Graph (STKG), the Multi-modal Mobility Representation first constructs a novel Spatial-Temporal Relational Graph (STRG). This graph is built using spatial-temporal dynamics embedded in STKG-fused mobility dynamics, and it supports multi-modal location fusion. Additionally, the Multi-modal Mobility Representation builds multi-level user preferences by leveraging textual semantics that range from coarse to fine granularity. (c) Multi-modal Trajectory Optimization is regularized by hierarchical semantic prediction and STKG-guided cross-modal alignment to incorporate multi-modal spatial-temporal knowledge.

4.1 Spatial-Temporal Knowledge Graph

High-order textual semantics alleviates long-tail location data sparsity and enrich the entity association dimensions of SpatioTemporal Knowledge Graph (STKG). Distinct from the existing works [26, 38], we are the first to inject textual semantics derived from Large Language Models (LLMs) into STKG, thereby obtaining hierarchical spatiotemporal dynamic relationships. We first applied DeepSeek-R1¹ to cluster location-based categorical texts, thereby obtaining 12 general human activity types. This process resulted in a three-level semantic hierarchy, ranging from coarse to fine: activity, category, and location. The prompt for activity generation is provided in Appendix A.1. This LLM-based approach not only enhances mapping accuracy but also addresses the challenges arising from divergent category definitions across different urban contexts.

Formally, a Hierarchical STKG is defined as a multi-relation graph $\mathcal{G} = (\mathcal{E}, \mathcal{R}, \mathcal{F})$, where \mathcal{E} is the set of entities, \mathcal{R} is the set of relations and $\mathcal{F} = \{(e^{\text{head}}, r, e^{\text{tail}})\}$, where $\text{head}, \text{tail} \in \mathcal{E}, r \in \mathcal{R}$. Each triplet $(e^{\text{head}}, r, e^{\text{tail}})$ denotes an edge in KG from head to tail with relation r . We consider users, locations, and their associated categories and activities as spatial-temporal entities to enhance knowledge capacity and characterize relations of entities as follows.

- **Functionality Knowledge.** Hierarchical relations r_f describe the mappings among multi-level entities (location, category, and activity): (p_i, r_f, c_j) and (c_j, r_f, a_k) .
- **Visit relation of Mobility Knowledge:** Visit relation r^t is defined as a user's interaction with a location, along with its associated categories and activities, represented by the triplets (u, r^t, p) , (u, r^t, c) , and (u, r^t, a) . Here, the temporal context r^t is discretized into 48 time slots.
- **Transition relation of Mobility Knowledge:** Transition relation r_t models entity transitions in trajectories between locations (p_i, r_t, p_j) , categories (c_i, r_t, c_j) , and activities (a_i, r_t, a_j) , capturing sequential behavior.

We pretrain STKG using TransE [1] and the resulting embeddings are then utilized in subsequent modules to construct the spatial-temporal relation graph, which is further adopted to fuse the multi-modal representations of locations.

4.2 Multi-modal Mobility Representation

4.2.1 Spatial-Temporal Relational Graph. We construct a data-driven Spatial-Temporal Relational Graph by leveraging entity similarity in the STKG, which establishes unified dynamic relationships for multi-modal data and effectively mitigates the issue of data sparsity. The similarity function of multi-level entities is computed by

$$\begin{aligned} \text{sim}(e_i, e_j) &= \exp(-d(e_i, e_j)), e \in \{p, c, a\}, \\ d(e_i, e_j) &= \|\text{ent}^{e_i} + r_t - \text{ent}^{e_j}\|, e \in \{p, c, a\}, \end{aligned} \quad (1)$$

where $\text{ent}^{k_i}, \text{ent}^{k_j}, r_t$ are obtained from the pretrained STKG. Using the hierarchical transition edge weights computed via Equation 1, we establish three mobility transition matrices $M^p \in N_p \times N_p$, $M^c \in N_c \times N_c$, $M^a \in N_a \times N_a$. N_c and N_a are the number of categories and activities, respectively.

¹<https://www.deepseek.com/>

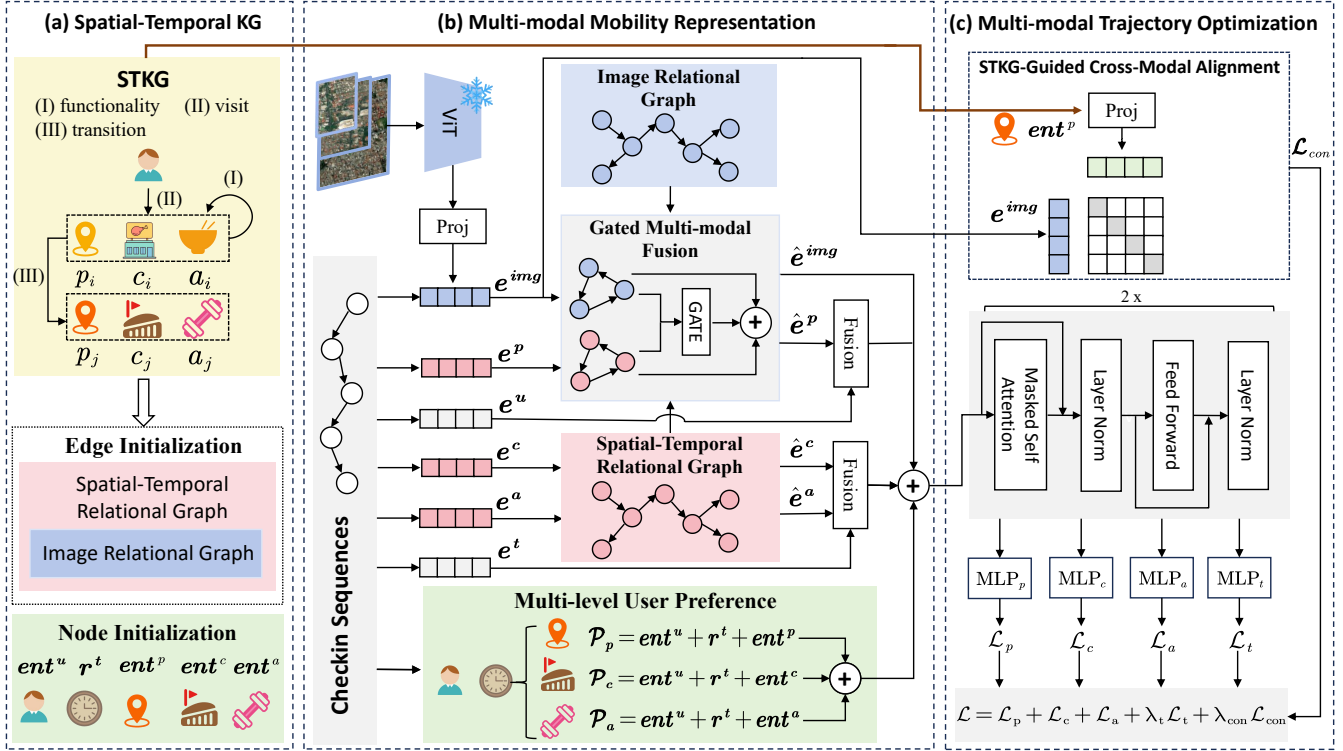


Figure 1: The illustration diagram of our proposed Multi-Modal Mobility representation (M³ob) framework. Among these, spatial-temporal knowledge graph, spatial-temporal relational graph, and image relational graph are responsible for modeling multi-modal dynamics, while gated multi-modal fusion and STKG-guided cross-modal alignment enable multi-modal alignment.

We further reduce useless graph edges by selecting from k nearest neighbors (k -NN), written as:

$$G_{i,j}^e = \begin{cases} M_{i,j}^e & \text{if Entity } e_j \in \mathcal{N}_k(e_i), e \in \{p, c, a\}, \\ 0, & \text{Otherwise} \end{cases} \quad (2)$$

where $\mathcal{N}_k(e_i)$ is the k nearest neighbors of different entities. The STRG is further normalized by dividing a diagonal matrix D_e of row-wise maximum values. The corresponding representations of different entities are obtained by GCN, written as:

$$\mathbf{Z}_e^{\text{fusion}} = \sigma(D_e^{-1} G^e \mathbf{Z}^e W), e \in \{p, c, a\}, \quad (3)$$

where \mathbf{Z}^e denotes the original one-hot embeddings of a type of entity, G^e is the corresponding STRG, W is a weight matrix, and $\sigma(\cdot)$ is the activation function.

Furthermore, we update the representations by integrating the spatial-temporal graph representations of both categories and activities with their original features through residual connections.

$$\hat{\mathbf{Z}}^e = \mathbf{Z}_e^{\text{fusion}} + \mathbf{Z}^e, e \in \{c, a\}, \quad (4)$$

4.2.2 Multi-scale Image Representation. In the real world, a direct correspondence exists between a remote sensing image and its geographic location, as such images capture the surrounding environmental semantics. Remote sensing images exhibit hierarchical semantics: lower zoom levels capture broader regional context, while higher levels provide finer-grained details. To effectively

leverage multi-scale representations, we first extract features from localized images at three zoom levels using pre-trained CLIP vision encoder (ViT). These features are then projected into the ID modality's semantic space via modality-specific MLP layers (Proj_h):

$$\mathbf{Z}^{\text{img}} = \sum_{h \in \mathcal{H}} \text{Proj}_h(\text{Image-Encoder}(p_{\text{img}}^h)). \quad (5)$$

To prevent catastrophic forgetting and reduce GPU memory requirements, we freeze the parameters of all pretrained image encoders during the following training tasks.

Image Relational Graph. We introduce mobility dynamic relationships into the remote sensing imagery to overcome the limitation of static graphs based on cosine similarity between images of previous methods [39]. To achieve this, we share the Spatial-Temporal-Relational Graph (STRG) structure of a location with its corresponding image to build an image relational graph G^{img} . The corresponding representations of image modality are obtained by GCN, written as:

$$\mathbf{Z}_{\text{img}}^{\text{fusion}} = \sigma(D_{\text{img}}^{-1} G^{\text{img}} \mathbf{Z}^{\text{img}} W), \quad (6)$$

where D_{img} also denotes the row-wise max diagonal matrix of G^{img} .

4.2.3 Gated Multi-modal Fusion. Cross-modal fusion of ID and image representations is essential for multi-modal interaction, but direct application of static weighting may induce modality conflicts. To address this issue, we employ a gated fusion mechanism that

dynamically adjusts the contribution of each modality. Specifically, we first concatenate $\mathbf{Z}_p^{\text{fusion}} \in \mathbb{R}^{N_p \times d}$ and $\mathbf{Z}_{\text{img}}^{\text{fusion}} \in \mathbb{R}^{N_p \times d}$, then apply a linear transformation followed by a Sigmoid activation to generate gate values $g \in \mathbb{R}^{N_p \times d}$ constrained within $[0, 1]$; finally, these gate values weight the two modalities:

$$\begin{aligned} g &= \text{Sigmoid}(W[\mathbf{Z}_p^{\text{fusion}} \parallel \mathbf{Z}_{\text{img}}^{\text{fusion}}] + b), \\ \mathbf{Z}^m &= g \odot \mathbf{Z}_p^{\text{fusion}} + (1 - g) \odot \mathbf{Z}_{\text{img}}^{\text{fusion}}, \end{aligned} \quad (7)$$

where $W \in \mathbb{R}^{d \times 2d}$ is a weight matrix, $b \in \mathbb{R}^d$ is a bias vector, \parallel denotes concatenation, and \odot is element-wise multiplication. We then perform residual weighting between the multi-modal graph representations \mathbf{Z}^m and the original image/ID modality representations respectively, written as:

$$\begin{aligned} \hat{\mathbf{Z}}^p &= \alpha \mathbf{Z}^m + (1 - \alpha) \mathbf{Z}^p, \\ \hat{\mathbf{Z}}^{\text{img}} &= \alpha \mathbf{Z}^m + (1 - \alpha) \mathbf{Z}^{\text{img}}, \end{aligned} \quad (8)$$

where \mathbf{Z}^p denotes the original one-hot embeddings of POI, α denotes a hyperparameter that controls the proportion of multi-modal graph fused information. This residual connection can effectively help avoid the degradation of cross-modal representations caused by the intra-modal noise.

4.2.4 Multi-level User Preference. To capture users' preferences for different levels of locations, we construct a multi-level user preference representation following the hierarchical knowledge of textual semantics, written as:

$$\mathcal{P}_{\text{multi}} = \mathcal{P}_p + \mathcal{P}_c + \mathcal{P}_a, \quad (9)$$

where the preference \mathcal{P}_k is computed by $\mathcal{P}_k = \text{ent}^u + r^t + \text{ent}^k, k \in \{p, c, a\}$, by summing the embeddings of the visit triplet $(\text{ent}^u, r^t, \text{ent}^k)$ from STKG. During the training process, we freeze all entity and relation representations to avoid preference forgetting while fine-tuning down-stream prediction tasks.

4.3 Multi-modal Trajectory Optimization

4.3.1 Hierarchical Regularization. The mobility sequence representation starts from a visit record of (u, p, t) and its associated category and activity following the hierarchical knowledge of textual semantics, written as:

$$\mathbf{Z}^r = f(\hat{\mathbf{Z}}^p, \mathbf{Z}^u) \parallel f(\hat{\mathbf{Z}}^c, \hat{\mathbf{Z}}^a, \mathbf{Z}^t) \parallel \mathcal{P}_{\text{multi}} \parallel \hat{\mathbf{Z}}^{\text{img}}, \quad (10)$$

where \mathbf{Z}^u denotes the one-hot encoded representation of user IDs and $f(\cdot) = \text{MLP}(\text{concat}(\cdot))$. A day is discretized into 48 time slots, each spanning 30 minutes, and temporal representations \mathbf{Z}^t are derived using Time2Vector [13] to capture temporal periodicity.

The corresponding representation S_{u_i} of the mobility sequence of user u_i is computed by $E_{S_{u_i}} = [\mathbf{Z}^{r_1}, \mathbf{Z}^{r_2}, \dots, \mathbf{Z}^{r_{|S_{u_i}|}}]$. The obtained representation matrix of the mobility sequence is then fed into the Transformer decoder to obtain the final representation, written as:

$$\hat{\mathbf{h}}_{|S_{u_i}|} = \text{Transformer}([\mathbf{Z}_1, \mathbf{Z}_2, \dots, \mathbf{Z}_{|S_{u_i}|}]), \quad (11)$$

where the Transformer computes the attention scores of the historical locations iteratively as $\text{softmax}(\frac{OK^T}{\sqrt{d}})V$.

By incorporating the next category, activity, and time as auxiliary tasks, prediction performance for the next location can be

enhanced. Therefore, we construct four MLP prediction heads to simultaneously perform four prediction tasks, written as:

$$\mathbf{y}_k = \text{MLP}_k(\hat{\mathbf{h}}_{S_{u_i}}), k \in \{p, c, a, t\}. \quad (12)$$

4.3.2 STKG-Guided Cross-Modal Alignment. To bridge the semantic gap between static multi-modal data and dynamic mobility behaviors, we enrich the static image representations with the spatial-temporal dynamics from the Hierarchical Spatial-Temporal Knowledge Graph (STKG). Specifically, we first input the location entity from the pretrained STKG and the image into two independent projection layers and align them in the same space.

$$\mathbf{Z}^{\text{KG}} = \text{Proj}_{\text{KG}}(\text{ent}^p), \quad (13)$$

where Proj_{KG} is a projection layer composed of a single layer MLP. The alignment loss between image-modal and STKG entity are computed in a global way, which treats the corresponding img_i and p_i as the positive sample and img_i and $p_j (j \neq i)$ as negative samples, written as:

$$\begin{aligned} \mathcal{L}_{\text{con}} = & -\frac{1}{N_p} \sum_{i=1}^{N_p} \log \left[\frac{\exp(\text{sim}(\mathbf{Z}_i^{\text{KG}}, \mathbf{Z}_i^{\text{img}}))}{\sum_{j=1}^{N_p} \exp(\text{sim}(\mathbf{Z}_i^{\text{KG}}, \mathbf{Z}_j^{\text{img}}))} \right. \\ & \left. + \log \frac{\exp(\text{sim}(\mathbf{Z}_i^{\text{img}}, \mathbf{Z}_i^{\text{KG}}))}{\sum_{j=1}^{N_p} \exp(\text{sim}(\mathbf{Z}_i^{\text{img}}, \mathbf{Z}_j^{\text{KG}}))} \right], \end{aligned} \quad (14)$$

where $\text{sim}(\cdot)$ denotes the inner product. Bidirectional contrastive learning can prevent modal collapse. Cross-modal alignment enhances the spatial-temporal dynamics of the image modality.

4.3.3 Training Objective. Finally, we adopt a multi-task learning approach to collaboratively optimize four prediction losses and cross-modal alignment losses to enhance the next location recommendation, our training objective integrates all previous loss functions, written as:

$$\mathcal{L} = \mathcal{L}_p + \mathcal{L}_c + \mathcal{L}_a + \lambda_t \mathcal{L}_t + \lambda_{\text{con}} \mathcal{L}_{\text{con}}, \quad (15)$$

where \mathcal{L}_p , \mathcal{L}_c and \mathcal{L}_a denote the cross-entropy losses for next location, next category and next activity prediction, respectively, and \mathcal{L}_t represents the mean squared error loss for next time prediction. $\lambda_t, \lambda_{\text{con}}$ is the weights of $\mathcal{L}_t, \mathcal{L}_{\text{con}}$, respectively.

5 Experiments

We conduct extensive experiments on real trajectory dataset of six cities to verify the performance of **M³ob** in next-location recommendation task. We aim to answer the following research questions:

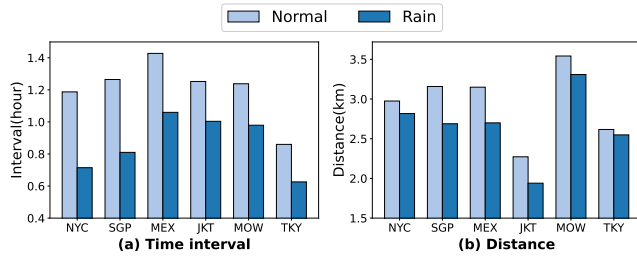
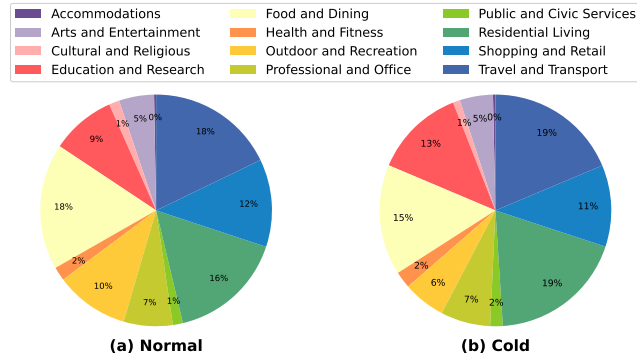
- **RQ1:** How does **M³ob** perform compared with other state-of-the-art methods for the next-location recommendation task?
- **RQ2:** How is the generalization capability of **M³ob** under abnormal scenarios like adverse weather and long-tail locations?
- **RQ3:** How does **M³ob** compare with baselines in efficiency?
- **RQ4:** How do different modules affect the prediction performance of **M³ob** across various mobility datasets?
- **RQ5:** How do hyper-parameter influence **M³ob**'s performance?

5.1 Experiment Setup

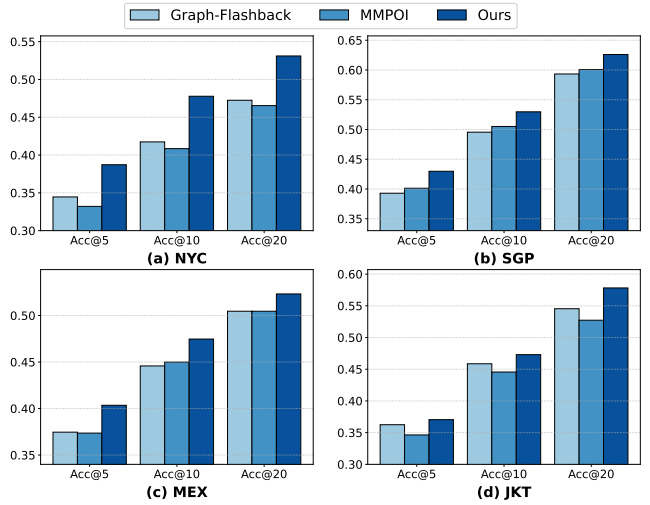
5.1.1 Datasets. To train and evaluate our model's performance, we conduct extensive experiments on trajectory datasets from six cities

Table 2: Basic statistics of mobility datasets.

Datasets	#User	#Loc	#Record	#Cat	#Traj
NYC	1,331	9,312	103,012	352	22,244
SGP	1,997	8,561	215,885	325	44,255
MEX	2,324	11,574	139,312	352	34,946
JKT	3,189	13,597	223,802	355	51,635
MOW	3,907	15,047	278,362	363	64,698
TKY	3,803	12,618	424,535	325	85,391

**Figure 2: Urban Variations in Time Intervals and Distances Between Normal and Rainy Weather.****Figure 3: Human Activity in Normal VS Cold Weather.**

sourced from Foursquare². We perform a general preprocessing step [28], filtering locations with fewer than 10 visits; defining all check-ins within a calendar day as a single trajectory; removing trajectories with fewer than 3 check-ins; and excluding inactive users with fewer than 5 trajectories. Each user’s trajectory is split chronologically: 80% training, 10% validation, and 10% test. Table 2 summarizes the statistics of the experimental datasets. Image representations are derived from 256×256-pixel satellite imagery acquired via ArcGIS³ at three granularities: coarse (zoom level 15), medium (zoom level 16), and fine (zoom level 17). Weather data are obtained from ERA5-Land⁴. Figure 2 compares the time intervals and geographical distances between consecutive locations in trajectories under rainy and sunny conditions across six cities. Figure 3

²<https://sites.google.com/site/yangdingqi/home/foursquare-dataset>³<https://server.arcgisonline.com/>⁴<https://cds.climate.copernicus.eu/datasets>**Figure 4: Prediction accuracy on rainy weather.**

compares the proportion of human activities on MOW under colder periods versus normal weather conditions.

5.1.2 Baselines. To validate **M³ob**’s effectiveness, we benchmark it against 11 state-of-the-art baselines. These comparative baselines are categorized into sequence-based methods [7, 8, 10, 28, 30, 41] and graph-based methods [25, 26, 38, 39, 43]. More details are provided in Appendix B.1.

5.1.3 Evaluation Metrics. We evaluate predictions using $\text{Acc}@k$, the standard location recommendation metric. This metric assesses whether the true next location appears in the top- k recommendations, effectively measuring system accuracy.

5.2 RQ1: Performance Comparison

Table 3 shows the performance of different baselines on 6 datasets. Our method consistently outperforms state-of-the-art baselines across all datasets, achieving average improvements of 3.71% at $\text{Acc}@5$, 3.70% at $\text{Acc}@10$, and 3.31% at $\text{Acc}@20$. Among sequence-based methods, LSTPM excels by explicitly modeling long- and short-term preferences, while MCLP struggles with sparse trajectory data and topic modeling fails to capture diverse user preferences. Graph-based methods like GETNext and Diff-POI show no improvement over sequence approaches: GETNext introduces noise via its Transition Attention Map, and Diff-POI underutilizes temporal sequences. Although Graph-Flashback and LoTNext leverage spatial-temporal knowledge graphs, they neglect real-world multi-modal information. MMPOI leads other graph-based methods but primarily uses multi-modal data for intra-modal similarity graphs and fails to leverage high-quality multi-modal explicit representations. See Appendix B.3 for hyperparameter search results of the latest baseline methods (MCLP, LoTNext).

5.3 RQ2: Generalization Analysis of **M³ob**

5.3.1 Performance Analysis on Adverse Weather. Human travel preferences shift significantly in rainy and cold weather [2, 5, 11]. As

Table 3: Performance comparison against *state-of-the-art* baseline methods. The best results are denoted by **bold font, and the second best ones are denoted by underline. Each model was trained five times independently with different random seeds, and the results are reported as mean \pm standard deviation.**

Method	NYC			SGP			MEX		
	Acc@5 (%)	Acc@10 (%)	Acc@20 (%)	Acc@5 (%)	Acc@10 (%)	Acc@20 (%)	Acc@5 (%)	Acc@10 (%)	Acc@20 (%)
Markov	29.10 \pm 0.00	33.80 \pm 0.00	35.71 \pm 0.00	32.15 \pm 0.00	39.52 \pm 0.00	45.24 \pm 0.00	23.72 \pm 0.00	27.93 \pm 0.00	30.58 \pm 0.00
LSTM	33.66 \pm 0.21	41.04 \pm 0.32	46.76 \pm 0.25	39.51 \pm 0.34	48.45 \pm 0.30	56.53 \pm 0.25	32.42 \pm 0.23	37.94 \pm 0.29	42.75 \pm 0.31
Deepmove	37.00 \pm 0.38	44.54 \pm 0.41	50.50 \pm 0.39	42.30 \pm 0.43	51.92 \pm 0.43	60.74 \pm 0.32	36.30 \pm 0.30	42.70 \pm 0.33	48.00 \pm 0.47
LSTPM	<u>38.54</u> \pm 0.53	<u>46.31</u> \pm 0.31	52.51 \pm 0.47	<u>43.22</u> \pm 0.19	52.91 \pm 0.19	61.89 \pm 0.15	<u>37.34</u> \pm 0.21	44.39 \pm 0.26	50.13 \pm 0.41
Flashback	37.37 \pm 0.26	45.34 \pm 0.25	51.68 \pm 0.21	41.97 \pm 0.16	51.46 \pm 0.19	60.12 \pm 0.14	36.33 \pm 0.19	43.07 \pm 0.10	48.85 \pm 0.11
MCLP	36.87 \pm 0.19	44.51 \pm 0.25	50.46 \pm 0.09	42.36 \pm 0.06	51.26 \pm 0.23	59.82 \pm 0.32	36.23 \pm 0.29	43.16 \pm 0.29	48.72 \pm 0.08
GETNEXT	34.58 \pm 0.18	42.01 \pm 0.30	48.34 \pm 0.41	40.90 \pm 0.13	48.93 \pm 0.13	56.35 \pm 0.24	30.95 \pm 0.12	36.99 \pm 0.23	41.98 \pm 0.32
Graph-Flashback	36.84 \pm 0.19	45.59 \pm 0.14	52.55 \pm 0.14	41.85 \pm 0.22	52.33 \pm 0.15	61.56 \pm 0.07	36.97 \pm 0.33	44.74 \pm 0.20	50.89 \pm 0.14
Diff-POI	29.22 \pm 0.17	39.30 \pm 0.19	46.50 \pm 0.17	29.75 \pm 0.12	40.98 \pm 0.11	51.05 \pm 0.21	29.93 \pm 0.56	38.45 \pm 0.27	44.65 \pm 0.20
MMPOI	36.71 \pm 0.24	45.86 \pm 0.08	<u>52.72</u> \pm 0.17	42.78 \pm 0.15	<u>53.41</u> \pm 0.16	<u>62.73</u> \pm 0.12	37.06 \pm 0.19	<u>44.86</u> \pm 0.15	<u>51.18</u> \pm 0.19
LoTNext	35.58 \pm 0.16	43.81 \pm 0.07	50.65 \pm 0.25	42.52 \pm 0.01	52.32 \pm 0.12	61.07 \pm 0.19	34.28 \pm 0.13	42.04 \pm 0.28	48.40 \pm 0.25
M³ob	39.91 \pm 0.17	48.59 \pm 0.07	54.96 \pm 0.25	45.82 \pm 0.13	55.99 \pm 0.08	64.99 \pm 0.13	38.96 \pm 0.16	46.56 \pm 0.12	52.95 \pm 0.22
Improv. %	3.55	4.92	4.25	6.02	4.83	3.60	4.34	3.79	3.46
Method	JKT			MOW			TKY		
	Acc@5 (%)	Acc@10 (%)	Acc@20 (%)	Acc@5 (%)	Acc@10 (%)	Acc@20 (%)	Acc@5 (%)	Acc@10 (%)	Acc@20 (%)
Markov	25.23 \pm 0.00	30.82 \pm 0.00	35.61 \pm 0.00	23.50 \pm 0.00	28.60 \pm 0.00	32.60 \pm 0.00	29.97 \pm 0.00	37.65 \pm 0.00	44.51 \pm 0.00
LSTM	31.63 \pm 0.22	39.53 \pm 0.23	47.74 \pm 0.17	31.96 \pm 0.20	38.06 \pm 0.29	43.38 \pm 0.36	36.84 \pm 0.24	44.07 \pm 0.45	51.05 \pm 0.62
Deepmove	35.56 \pm 0.40	44.30 \pm 0.47	53.40 \pm 0.40	36.46 \pm 0.43	43.78 \pm 0.66	49.98 \pm 0.72	41.34 \pm 0.63	49.98 \pm 0.54	57.77 \pm 0.60
LSTPM	<u>36.46</u> \pm 0.17	45.36 \pm 0.17	54.25 \pm 0.24	37.17 \pm 0.37	45.18 \pm 0.27	51.84 \pm 0.29	<u>43.75</u> \pm 0.10	52.18 \pm 0.13	59.61 \pm 0.11
Flashback	35.36 \pm 0.07	44.03 \pm 0.19	52.90 \pm 0.12	36.33 \pm 0.11	43.07 \pm 0.11	48.85 \pm 0.14	39.35 \pm 0.12	48.16 \pm 0.11	56.03 \pm 0.05
MCLP	35.02 \pm 0.09	43.38 \pm 0.10	51.96 \pm 0.23	36.42 \pm 0.14	44.24 \pm 0.25	50.63 \pm 0.19	40.96 \pm 0.07	49.29 \pm 0.13	56.84 \pm 0.13
GETNEXT	32.10 \pm 0.27	39.32 \pm 0.34	46.93 \pm 0.55	33.55 \pm 0.13	40.35 \pm 0.28	46.13 \pm 0.26	38.91 \pm 0.30	47.14 \pm 0.31	54.70 \pm 0.25
Graph-Flashback	36.39 \pm 0.09	<u>46.06</u> \pm 0.18	<u>55.42</u> \pm 0.15	37.21 \pm 0.19	45.44 \pm 0.12	52.42 \pm 0.17	40.50 \pm 0.13	49.95 \pm 0.11	58.11 \pm 0.08
Diff-POI	27.95 \pm 0.19	36.85 \pm 0.09	45.55 \pm 0.11	31.33 \pm 0.32	40.33 \pm 0.26	47.98 \pm 0.18	29.87 \pm 0.09	39.76 \pm 0.09	48.47 \pm 0.05
MMPOI	35.74 \pm 0.22	45.53 \pm 0.20	54.82 \pm 0.21	<u>38.02</u> \pm 0.17	<u>46.60</u> \pm 0.14	<u>53.63</u> \pm 0.20	42.66 \pm 0.12	<u>52.38</u> \pm 0.11	<u>60.69</u> \pm 0.11
LoTNext	34.85 \pm 0.07	44.56 \pm 0.12	54.20 \pm 0.08	35.70 \pm 0.12	44.31 \pm 0.14	51.51 \pm 0.15	40.79 \pm 0.08	50.01 \pm 0.05	58.46 \pm 0.08
M³ob	37.61 \pm 0.11	47.53 \pm 0.22	57.31 \pm 0.20	39.25 \pm 0.09	47.91 \pm 0.12	55.11 \pm 0.13	44.61 \pm 0.15	53.76 \pm 0.09	62.12 \pm 0.10
Improv. %	3.15	3.19	3.41	3.24	2.81	2.76	1.97	2.63	2.36

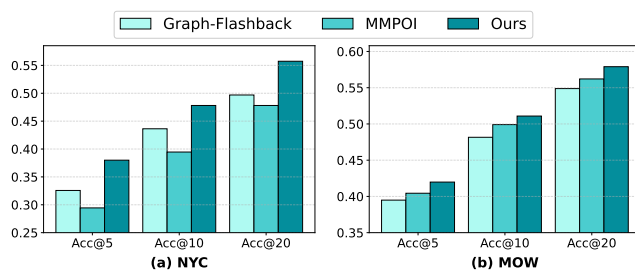


Figure 5: Prediction accuracy on cold weather.

shown in Figure 2, analysis of trajectory data from six cities shows that during rain, average time intervals and spatial distances decreased by 28.2% and 9.7% respectively compared to sunny conditions. Movement speed increased, indicating a preference for visiting nearer locations and greater use of vehicles. NYC and MOW, situated at higher latitudes, are frequently affected by cold

weather. As shown in Figure 3, in cold weather, people favor indoor activities, reducing trips for dining and shopping. Such specific weather conditions challenge the generalization of mobility models in sparse scenarios. As shown in Figure 4 and Figure 5, our method significantly outperforms Graph-Flashback and MMPOI in location recommendation under both rainy and cold weather. This consistent advantage across datasets confirms our approach's generalization in adverse weather. This is because the remote sensing image module in our method enriches the environmental semantics of locations, while the text semantics of LLM captures high-level differences in human activities. Additionally, the unified STRG and the STKG-guided cross-modal alignment enhance the spatiotemporal knowledge across modalities, enabling the capture of dynamic shifts in human behavior under adverse weather conditions.

5.3.2 Performance Analysis on Long-tail Locations. Long-tail locations (frequency < 20) pose significant challenges in mobility prediction due to the lack of collaborative signals. Our proposed **M³ob** addresses this by leveraging frequency-agnostic multi-modal

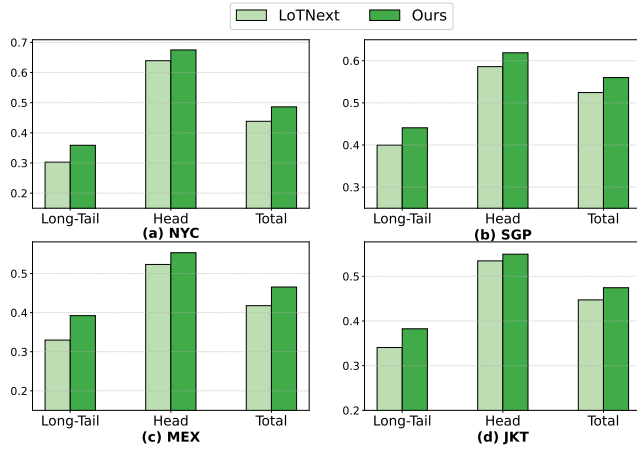


Figure 6: Prediction accuracy on long-tail locations. The performance is measured using Acc@10.

Table 4: Model efficiency comparison.

Method	NYC			SGP		
	Memory	Train	Infer	Memory	Train	Infer
Deepmove	1,141M	1.20	1.27	1,579M	2.45	2.50
LSTPM	1,781M	23.42	3.20	1,609M	47.80	5.88
Graph-Flashback	3,913M	0.52	0.83	3,783M	1.20	1.53
LoTNext	2,211M	2.35	1.08	1,323M	5.13	2.22
MMPOI	5,263M	1.53	1.25	5,519M	3.43	2.40
M³ob	4,931M	0.43	0.33	5,055M	1.02	0.80

Note: M (megabyte), Train/Infer (minute).

data. As shown in Figure 6, our method consistently outperforms LoTNext (a long-tail adjustment framework) in predicting both head and tail locations. The performance of LoTNext is limited by the sparse trajectory data and inherent data biases, whereas our approach enriches information for long-tail locations by leveraging real-world textual and visual modalities. Moreover, through a shared spatial-temporal relational graph, our method endows different modalities with dynamic spatial-temporal representations, enabling effective semantic transfer from head locations to tail ones.

5.4 RQ3: Efficiency Evaluation

As shown in Table 4, our method demonstrates superior training and inference efficiency over competitive baselines on NYC and SGP datasets: Among sequence-based methods, LSTPM incurs substantially higher training/validation time by serially processing each historical trajectory; for graph-based methods, LoTNext requires additional time overhead per iteration due to graph denoising operations. Furthermore, despite utilizing multi-modal data, our lightweight model construction introduces little additional memory overhead compared to unimodal methods.

5.5 RQ4: Ablation Study

To evaluate the effectiveness of different modules, we constructed six variants of **M³ob** in our ablation study. As shown in Table 5, the

Table 5: Ablation analysis of M³ob. The recommendation performance is measured using Acc@10 (%).

Variants	NYC	SGP	MEX	JKT
Multi-modal Data				
w/o Img	46.29 ± 0.13	53.94 ± 0.09	43.92 ± 0.33	45.51 ± 0.21
w/o Text	48.16 ± 0.11	55.61 ± 0.07	46.19 ± 0.25	47.12 ± 0.26
Multi-modal Fusion				
w/o IRG	48.30 ± 0.16	55.66 ± 0.24	46.24 ± 0.13	47.28 ± 0.15
w/o STRG	48.02 ± 0.11	55.35 ± 0.11	45.69 ± 0.10	47.02 ± 0.28
w/o MUP	48.31 ± 0.13	55.69 ± 0.16	46.15 ± 0.19	47.29 ± 0.20
Multi-modal Alignment				
w/o CMA	47.87 ± 0.18	55.65 ± 0.26	46.08 ± 0.08	47.16 ± 0.10
M³ob	48.59 ± 0.07	55.99 ± 0.08	46.56 ± 0.12	47.53 ± 0.22

results demonstrate the importance of our multi-modal integration and alignment designs. The variants are analyzed as follows:

- w/o Img: Removing the remote sensing image modality and cross-modal alignment leads to a clear performance drop (-4.58%), as images are capable of effectively enriching the spatial hierarchy and environmental semantic information of locations.
- w/o Text: Excluding high-level textual semantics from the knowledge graph and related loss functions reduces performance, since text helps cluster locations with similar categories and enriches hierarchical semantic representation.
- w/o IRG: Removing the image relation graph (IRG), which links mobility dynamic behavior to static images, causes a decline by widening the semantic gap between behavior and static image.
- w/o STRG: When the spatial-temporal relational graph (STRG) is excluded, the IRG is also removed simultaneously—this is because the IRG is derived from the STRG. The STRG is capable of modeling dynamic relationships between multiple modalities and mitigating the sparsity issue; consequently, the model’s performance decreases (-1.31%) after this module is removed.
- w/o MUP: Omitting multi-level user preferences (MUP), which capture time-aware user interests across location semantics, results in observable performance degradation.
- w/o CMA: Eliminating the cross-modal alignment (CMA), which infuses images with spatial-temporal dynamics from the knowledge graph, also leads to a performance drop.

5.6 RQ5: Hyper-parameter Sensitivity

Figure 7 illustrates variation in prediction accuracy of **M³ob** with the multi-modal representation fusion weight α . Our hyperparameter search over α in the range [0.0, 0.2, 0.4, 0.6, 0.8, 1.0] reveals that performance significantly degrades without multi-modal graph representations ($\alpha = 0$), underscoring critical importance of spatial-temporal graph fusion; notably, omitting multi-modal residual connections ($\alpha = 1$) leads to a marked performance decline on four datasets, indicating these residuals effectively mitigate information loss across modalities. Furthermore, a fusion weight of $\alpha = 0.8$

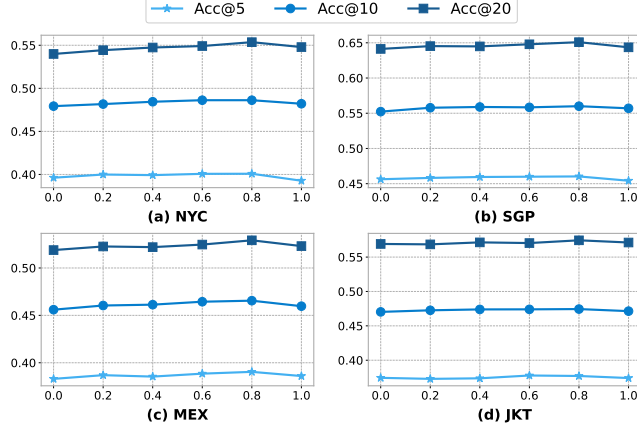


Figure 7: Effect of the graph fusion weight α .

consistently yields near-optimal results across all datasets. Hyper-parameter sensitivity experiments for K-NN on STRG and multitask loss weights can be found in Appendix B.4.

6 Conclusion

In this study, we introduce **M³ob**, a multi-modal fusion framework that leverages spatial-temporal knowledge to integrate human mobility dynamics with multi-modal representations, build a united STRG for multi-modal and implements STKG-guided cross-modal contrastive alignment. Our method exhibits strong generalization ability, as demonstrated by extensive comparative experiments conducted across both normal and abnormal scenarios—especially under adverse weather and long-tail locations. Benefiting from its lightweight design, the method also boasts high inference efficiency. Furthermore, ablation studies validate the contributions of different modules within our framework. In the future, we will explore dynamic scenarios for multi-modal mobility prediction to enhance the emergency management capabilities of decision-makers. Another promising direction is to investigate the interpretable human mobility paradigm by guiding the mobility of LLMs agents with their perceptual multi-modal knowledge.

References

- [1] Antoine Bordes, Nicolas Usunier, Alberto Garcia-Duran, Jason Weston, and Oksana Yakhnenko. 2013. Translating embeddings for modeling multi-relational data. *Advances in neural information processing systems* 26 (2013).
- [2] Vanessa S Brum-Bastos, Jed A Long, and Urška Demšar. 2018. Weather effects on human mobility: a study using multi-channel sequence analysis. *Computers, Environment and Urban Systems* 71 (2018), 131–152.
- [3] Wei Chen, Huaiyu Wan, Shengnan Guo, Haoyu Huang, Shaojie Zheng, Jiamu Li, Shuoqiao Lin, and Youfang Lin. 2022. Building and exploiting spatial-temporal knowledge graph for next POI recommendation. *Knowledge-Based Systems* 258 (2022), 109951.
- [4] Xi Chen, Yangsiyi Liu, Yuehai Wang, and Jianyi Yang. 2021. Cmbf: Cross-modal-based fusion recommendation algorithm. *Sensors* 21, 16 (2021), 5275.
- [5] Mario Cools, Elke Moons, Lieve Creemers, and Geert Wets. 2010. Changes in travel behavior in response to weather conditions: do type of weather and trip purpose matter? *Transportation Research Record* 2157, 1 (2010), 22–28.
- [6] Chenghua Duan, Wei Fan, Wei Zhou, Hu Liu, and Junhao Wen. 2023. Clsprec: Contrastive learning of long and short-term preferences for next poi recommendation. In *CIKM*. 473–482.
- [7] Jie Feng, Yong Li, Chao Zhang, Funing Sun, Fanchao Meng, Ang Guo, and Depeng Jin. 2018. Deepmove: Predicting human mobility with attentional recurrent networks. In *WWW*. 1459–1468.
- [8] Sébastien Gambs, Marc-Olivier Killijian, and Miguel Núñez del Prado Cortez. 2012. Next place prediction using mobility markov chains. In *Proceedings of the first workshop on measurement, privacy, and mobility*. 1–6.
- [9] Haoyu Han, Mengdi Zhang, Min Hou, Fuzheng Zhang, Zhongyuan Wang, Enhong Chen, Hongwei Wang, Jianhui Ma, and Qi Liu. 2020. STGCN: a spatial-temporal aware graph learning method for POI recommendation. In *ICDM*. IEEE, 1052–1057.
- [10] Sepp Hochreiter and Jürgen Schmidhuber. 1997. Long short-term memory. *Neural computation* 9, 8 (1997), 1735–1780.
- [11] Teerayut Horanont, Santi Phithakkitnukoon, Tuck W Leong, Yoshihide Sekimoto, and Ryosuke Shibasaki. 2013. Weather effects on the patterns of people's everyday activities: a study using GPS traces of mobile phone users. *PLoS one* 8, 12 (2013), e81153.
- [12] Nan Jiang, Haitao Yuan, Jianing Si, Minxiao Chen, and Shangguang Wang. 2024. Towards effective next POI prediction: Spatial and semantic augmentation with remote sensing data. In *ICDE*. IEEE, 5061–5074.
- [13] Seyed Mehran Kazemi, Rishab Goel, Sepehr Eghbali, Janahan Ramanan, Jaspreet Sahota, Sanjay Thakur, Stella Wu, Cathal Smyth, Pascal Poupart, and Marcus Brubaker. 2019. Time2vec: Learning a vector representation of time. *arXiv preprint arXiv:1907.05321* (2019).
- [14] Nicholas D Lane, Dimitrios Lymberopoulos, Feng Zhao, and Andrew T Campbell. 2010. Haporl: context-based local search for mobile phones using community behavioral modeling and similarity. In *Proceedings of the 12th ACM international conference on Ubiquitous computing*. 109–118.
- [15] Nicholas Lim, Bryan Hooi, See-Kiong Ng, Yong Liang Goh, Renrong Weng, and Rui Tan. 2022. Hierarchical multi-task graph recurrent network for next poi recommendation. In *SIGIR*. 1133–1143.
- [16] Chang Liu, Xiaoguang Li, Guohao Cai, Zhenhua Dong, Hong Zhu, and Lifeng Shang. 2021. Noninvasive self-attention for side information fusion in sequential recommendation. In *AAAI*, Vol. 35. 4249–4256.
- [17] Huizhi Liu, Chen Li, and Lihua Tian. 2022. Multi-modal graph attention network for video recommendation. In *CCET*. IEEE, 94–99.
- [18] Hongtao Liu, Fangzhao Wu, Wenjun Wang, Xianchen Wang, Pengfei Jiao, Chuhu Wu, and Xing Xie. 2019. NRPA: Neural recommendation with personalized attention. In *SIGIR*. 1233–1236.
- [19] Qidong Liu, Jiaxi Hu, Yutian Xiao, Xiangyu Zhao, Jingtong Gao, Wanyu Wang, Qing Li, and Jiliang Tang. 2024. Multimodal recommender systems: A survey. *Comput. Surveys* 57, 2 (2024), 1–17.
- [20] Shang Liu, Zhenzhong Chen, Hongyi Liu, and Xinghai Hu. 2019. User-video co-attention network for personalized micro-video recommendation. In *WWW*. 3020–3026.
- [21] Xin Liu, Yong Liu, and Xiaoli Li. 2016. Exploring the context of locations for personalized location recommendations. In *IJCAI*. 1188–1194.
- [22] Yifan Liu, Kangning Zhang, Xiangyuan Ren, Yanhua Huang, Jiarui Jin, Yingjie Qin, Ruilong Su, Ruiven Xu, Yong Yu, and Weinan Zhang. 2024. AlignRec: Aligning and Training in Multimodal Recommendations. In *CIKM*. 1503–1512.
- [23] Yingtao Luo, Qiang Liu, and Zhaocheng Liu. 2021. Stan: Spatio-temporal attention network for next location recommendation. In *WWW*. 2177–2185.
- [24] Yifang Qin, Yifan Wang, Fang Sun, Wei Ju, Xuyang Hou, Zhe Wang, Jia Cheng, Jun Lei, and Ming Zhang. 2023. DisenPOI: Disentangling sequential and geographical influence for point-of-interest recommendation. In *WSDM*. 508–516.
- [25] Yifang Qin, Hongjun Wu, Wei Ju, Xiao Luo, and Ming Zhang. 2023. A diffusion model for poi recommendation. *ACM Transactions on Information Systems* 42, 2 (2023), 1–27.
- [26] Xuan Rao, Lisi Chen, Yong Liu, Shuo Shang, Bin Yao, and Peng Han. 2022. Graph-flashback network for next location recommendation. In *KDD*. 1463–1471.
- [27] Xuan Rao, Renhe Jiang, Shuo Shang, Lisi Chen, Peng Han, Bin Yao, and Panos Kalnis. 2024. Next point-of-interest recommendation with adaptive graph contrastive learning. *IEEE Transactions on Knowledge and Data Engineering* (2024).
- [28] Ke Sun, Tieyun Qian, Tong Chen, Yile Liang, Quoc Việt Hung Nguyen, and Hongzhi Yin. 2020. Where to go next: Modeling long-and short-term user preferences for point-of-interest recommendation. In *AAAI*, Vol. 34. 214–221.
- [29] Rui Sun, Xuezhi Cao, Yan Zhao, Junchen Wan, Kun Zhou, Fuzheng Zhang, Zhongyuan Wang, and Kai Zheng. 2020. Multi-modal knowledge graphs for recommender systems. In *CIKM*. 1405–1414.
- [30] Tianao Sun, Ke Fu, Weiming Huang, Kai Zhao, Yongshun Gong, and Meng Chen. 2024. Going where, by whom, and at what time: Next location prediction considering user preference and temporal regularity. In *KDD*. 2784–2793.
- [31] Zhihui Tao, Yinwei Wei, Xiang Wang, Xiangnan He, Xianglin Huang, and Tat-Seng Chua. 2020. Mgat: Multimodal graph attention network for recommendation. *Information Processing & Management* 57, 5 (2020), 102277.
- [32] Qifan Wang, Yinwei Wei, Jianhua Yin, Jianlong Wu, Xuemeng Song, and Liqiang Nie. 2021. Dualgnn: Dual graph neural network for multimedia recommendation. *IEEE Transactions on Multimedia* 25 (2021), 1074–1084.
- [33] Yuequn Wang, Liyan Dong, Hao Zhang, Xintao Ma, Yongli Li, and Minghui Sun. 2020. An enhanced multi-modal recommendation based on alternate training with knowledge graph representation. *Ieee Access* 8 (2020), 213012–213026.
- [34] Zhaobo Wang, Yanmin Zhu, Chunyang Wang, Wenze Ma, Bo Li, and Jiadi Yu. 2023. Adaptive graph representation learning for next POI recommendation. In *SIGIR*. 393–402.
- [35] Yinwei Wei, Xiang Wang, Liqiang Nie, Xiangnan He, and Tat-Seng Chua. 2020. Graph-refined convolutional network for multimedia recommendation with implicit feedback. In *Proceedings of the 28th ACM international conference on multimedia*. 3541–3549.
- [36] Yinwei Wei, Xiang Wang, Liqiang Nie, Xiangnan He, Richang Hong, and Tat-Seng Chua. 2019. MMGCN: Multi-modal graph convolution network for personalized recommendation of micro-video. In *Proceedings of the 27th ACM international conference on multimedia*. 1437–1445.
- [37] Anna Wu and Xiaolong Zhang. 2011. Location-based information fusion for mobile navigation. In *Proceedings of the 13th international conference on Ubiquitous computing*. 593–594.
- [38] Xiaohang Xu, Renhe Jiang, Chuang Yang, Kaoru Sezaki, et al. 2024. Taming the long tail in human mobility prediction. *Advances in Neural Information Processing Systems* 37 (2024), 54748–54771.
- [39] Yang Xu, Gao Cong, Lei Zhu, and Lizhen Cui. 2024. MMPOI: A Multi-Modal Content-Aware Framework for POI Recommendations. In *WWW*. 3454–3463.
- [40] Xiaodong Yan, Tengwei Song, Yifeng Jiao, Jianshan He, Jiaotuan Wang, Ruopeng Li, and Wei Chu. 2023. Spatio-temporal hypergraph learning for next POI recommendation. In *SIGIR*. 403–412.
- [41] Dingqi Yang, Benjamin Fankhauser, Paolo Rosso, and Philippe Cudré-Mauroux. 2020. Location prediction over sparse user mobility traces using rnns. In *Proceedings of the twenty-ninth international joint conference on artificial intelligence*. 2184–2190.
- [42] Dingqi Yang, Daqing Zhang, Zhiyong Yu, and Zhiwen Yu. 2013. Fine-grained preference-aware location search leveraging crowdsourced digital footprints from LBSNs. In *Proceedings of the 2013 ACM international joint conference on Pervasive and ubiquitous computing*. 479–488.
- [43] Song Yang, Jiamou Liu, and Kaiqi Zhao. 2022. GETNext: trajectory flow map enhanced transformer for next POI recommendation. In *SIGIR*. 1144–1153.
- [44] Feiyu Yin, Yong Liu, Zhiqi Shen, Lisi Chen, Shuo Shang, and Peng Han. 2023. Next POI recommendation with dynamic graph and explicit dependency. In *AAAI*, Vol. 37. 4827–4834.
- [45] Jia-Dong Zhang, Chi-Yin Chow, and Yanhua Li. 2014. Lore: Exploiting sequential influence for location recommendations. In *SIGSPATIAL*. 103–112.
- [46] Pengpeng Zhao, Anjing Luo, Yanchi Liu, Jiajie Xu, Zhixu Li, Fuzhen Zhuang, Victor S Sheng, and Xiaofang Zhou. 2020. Where to go next: A spatio-temporal gated network for next poi recommendation. *IEEE Transactions on Knowledge and Data Engineering* 34, 5 (2020), 2512–2524.
- [47] Hongyu Zhou, Xin Zhou, Zhiwei Zeng, Lingzi Zhang, and Zhiqi Shen. 2023. A comprehensive survey on multimodal recommender systems: Taxonomy, evaluation, and future directions. *arXiv preprint arXiv:2302.04473* (2023).
- [48] Xin Zhou, Hongyu Zhou, Yong Liu, Zhiwei Zeng, Chunyan Miao, Pengwei Wang, Yuan You, and Feijun Jiang. 2023. Bootstrap latent representations for multimodal recommendation. In *WWW*. 845–854.

A Method Details.

A.1 LLM Prompt for Location Hierarchy.

The prompt used for generating Activity labels from Category data is shown as Figure 8. Based on the categorical text descriptions of locations, we employ a large language model to infer 12 generic types of human activities.

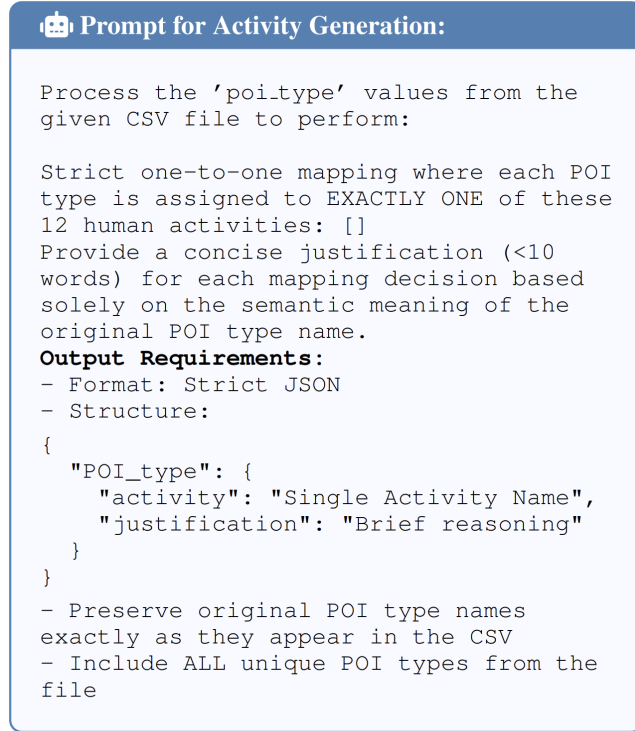


Figure 8: Category → Activity Prompt.

B Experiments.

B.1 Baselines.

To validate the effectiveness of **M³ob**, we benchmark it against 11 state-of-the-art baselines. These comparative baselines are categorized into sequence-based methods and graph-based methods.

1) Sequence-based model

- Markov [8]: It regards all visited locales as states, and constructs a transition matrix to capture the first-order transition probabilities between them.
- LSTM [10]: LSTM is a sophisticated variant of RNN, designed to adeptly manage sequential data.
- Deepmove [7]: It employs the attention mechanism to more effectively leverage historical data and contextual information during prediction.
- LSTPM [28]: It proposes using non-local networks and geographically dilated RNNs to model long- and short-term preferences.
- Flashback [41]: It employs the flashback mechanism to address historical trajectories.

- MCLP [30]: It employs thematic modeling to extract users' historical locational preferences and generates arrival time embeddings as the context for location recommendation through a multi-head attention mechanism.

2) Graph-based model

- GETNEXT [43]: It employs trajectory flow graph to capture the general movement patterns of users.
- Graph-Flashback [26]: Based on the spatial-temporal knowledge graph, enhance location representation by utilizing the temporal and spatial relationships between locations.
- Diff-POI [25]: It harnesses two graphs to extract spatial-temporal representations, and introduces a diffusion-based sampling strategy to investigate users' spatial preferences.
- MMPOI [39]: It leverages intra-modal cosine similarity to construct a multi-modal graph, thereby enriching location representation.
- LoTNext [38]: It proposes long-tailed graph adjustment and a long-tailed loss adjustment module to enhance long-tailed location prediction.

B.2 Implementation Details.

All experiments are performed on a single NVIDIA RTX 4090. We utilize Adam as the optimizer, with an initial learning rate set to 1e-4 and the L2 regularization penalty set to 1e-3. For the image encoder, we adopt CLIP's pre-trained image encoder (ViT-B-32). For Transformer, we stack two layers of encoders with a dropout of 0.3 and set the number of attention heads to 4 to run 75 epochs with batch size 128. We search for ID dimension from {128, 256, 512}. It is worth noting that we set the time loss and alignment loss weights to 10 and 1 respectively to match the scale of location and category losses. Additionally, we set the weights for the graph fusion representation to 0.8. For a fair comparison, we optimized each baseline's parameters as per their papers and recorded the mean and standard deviation across five random seeds.

B.3 Hyperparameter Search of Baselines.

Given their status as the latest sequence-based model (MCLP) and graph-based model (LoTNext) among our baseline comparisons, we conducted comprehensive grid hyperparameter search experiments for both methods. The results of these searches for selected parameters on the NYC and SGP datasets are presented in Table 6.

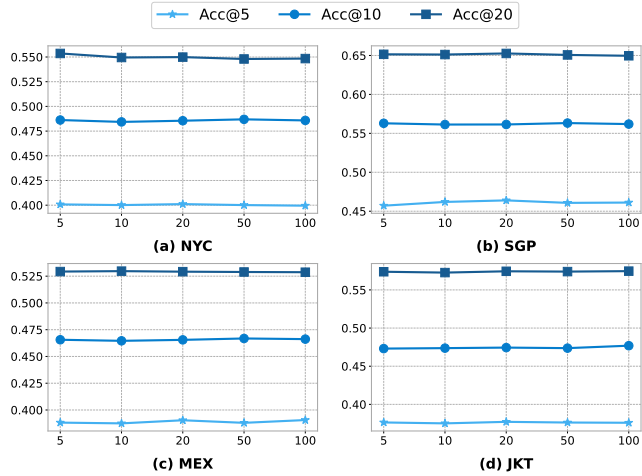
Despite extensive hyperparameter tuning, we observe that both methods continue to underperform prior work (e.g., LSTPM and Graph-Flashback). This performance gap occurs because MCLP was evaluated on datasets with lower sparsity than ours; their approach performs best with denser trajectory data. Furthermore, we identified a data leakage issue in the publicly released LoTNext code, where the Transformer module lacked temporal masking during inference. We confirmed this flaw via email correspondence with the authors and subsequently added masking to LoTNext in our experiments to ensure fair comparison.

B.4 More Parameter Analysis.

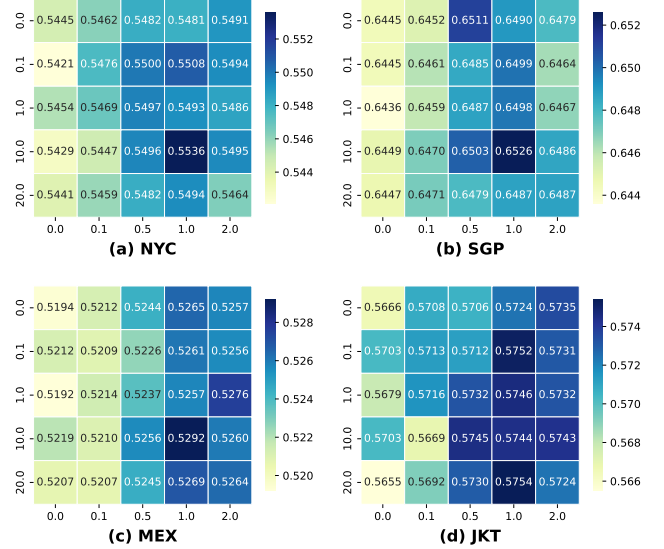
B.4.1 K-NN for Spatial-Temporal Relational Graph. Figure 9 demonstrates the prediction accuracy variation of **M³ob** with respect to the neighborhood size parameter k in the KNN-sparsified graph.

Table 6: Hyperparameter grid search results for MCLP and LoTNext on random seed 42.

MCLP	NYC			SGP		
	[batch, lr, dim]	Acc@5	Acc@10	Acc@20	Acc@5	Acc@10
[64,1e-4,128]	0.3675	0.4423	0.5012	0.4142	0.5073	0.5930
[64,1e-4,256]	0.3701	0.4462	0.5079	0.4224	0.5124	0.5976
[64,1e-3,128]	0.3488	0.4261	0.4890	0.4053	0.4957	0.5837
[64,1e-3,256]	0.3433	0.4204	0.4873	0.4041	0.4980	0.5818
[128,1e-4,128]	0.3647	0.4392	0.5029	0.4152	0.5070	0.5906
[128,1e-4,256]	0.3591	0.4314	0.4841	0.4225	0.5127	0.5976
[128,1e-3,128]	0.3574	0.4316	0.4911	0.4041	0.4984	0.5833
[128,1e-3,256]	0.3528	0.4291	0.4935	0.4006	0.4931	0.5770
[256,1e-4,128]	0.3659	0.4405	0.4975	0.4163	0.5078	0.5920
[256,1e-4,256]	0.3705	0.4458	0.5070	0.4244	0.5159	0.6019
[256,1e-3,128]	0.3553	0.4350	0.4907	0.4067	0.5016	0.5840
[256,1e-3,256]	0.3565	0.4352	0.4986	0.4010	0.4946	0.5774
LoTNext						
[batch, lr, dim]	NYC			SGP		
	Acc@5	Acc@10	Acc@20	Acc@5	Acc@10	Acc@20
[16,1e-4,128]	0.3549	0.4229	0.4796	0.4198	0.5118	0.5974
[16,1e-4,256]	0.3565	0.4338	0.4900	0.4273	0.5210	0.6062
[16,1e-3,128]	0.3560	0.4383	0.5083	0.4147	0.5158	0.6054
[16,1e-3,256]	0.3529	0.4386	0.5106	0.4133	0.5163	0.6118
[32,1e-4,128]	0.3516	0.4241	0.4760	0.4215	0.5178	0.6025
[32,1e-4,256]	0.3608	0.4348	0.4903	0.4228	0.5195	0.6058
[32,1e-3,128]	0.3575	0.4364	0.4986	0.4261	0.5244	0.6132
[32,1e-3,256]	0.3490	0.4283	0.4963	0.4224	0.5218	0.6089
[128,1e-4,128]	0.3517	0.4202	0.4765	0.4207	0.5186	0.6028
[128,1e-4,256]	0.3591	0.4314	0.4841	0.4268	0.5233	0.6078
[128,1e-3,128]	0.3421	0.4137	0.4774	0.4161	0.5083	0.5918
[128,1e-3,256]	0.3528	0.4291	0.4935	0.4219	0.5187	0.6059

**Figure 9: Effect of the k of k -NN for spatial-temporal Relational Graph.**

Our hyperparameter search over $k \in \{5, 10, 20, 50, 100\}$ reveals distinct patterns: For SGP, MEX and JKT, accuracy initially increases with larger k values and saturates at $k = 20$ as incorporating more

**Figure 10: Effect of the weights of multitask loss. The performance is measured using Acc@20.**

spatial-temporally relevant neighbors enriches multi-modal representations of locations; beyond this point, performance slightly declines due to noise introduced by weakly correlated neighbors. Conversely, for NYC, optimal accuracy is achieved at $k = 5$ with no significant improvement at larger values, which stems from extreme data sparsity—characterized by low average visit frequencies and abundant long-tail locations possessing few strongly associated neighbors.

B.4.2 Multitask Loss Weights. To analyze the impact of multi-task loss weights on the performance of our method, we searched for the alignment loss weight λ_{con} within the range $[0, 0.1, 0.5, 1, 2]$ and the temporal prediction loss weight λ_t within $[0, 0.1, 1, 10, 20]$. Figure 10 shows how the performance of our method varies with changes in the multi-task loss weights, where the x-axis represents λ_{con} and the y-axis represents λ_t . We observe that removing either the temporal loss or the alignment loss leads to a degradation in the performance of our method. Additionally, excessively high weights for both losses will cause an imbalance in the multi-task loss, resulting in performance degradation. Across the four datasets, $\lambda_t = 10$ and $\lambda_{\text{con}} = 1$ are found to be favorable values.

B.5 Impact of Scaling Ratio on Remote Sensing.

Remote sensing images with different scaling ratios exhibit distinct spatial structural semantics: high-scaling-ratio images contain more fine-grained information, while low-scaling-ratio ones have a larger receptive field. As shown in Figure 11, we compared the location recommendation performance of two cities with distinct morphological characteristics, using coarse-, medium-, fine-grained remote sensing images, and the multi-scale remote sensing images adopted in our framework as image modal representations respectively. We found that for NYC, a city with concentrated functional zones and large spatial scales, coarse-grained remote sensing images can

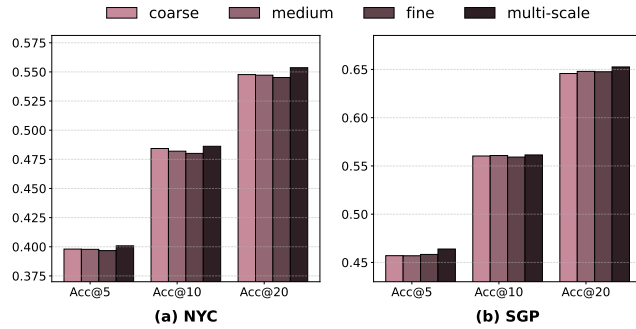


Figure 11: Effect of scaling ratio on remote sensing.

capture macro functional zone features and achieve the best performance. For SGP, a city with mixed functions and compact spaces, medium/fine-grained remote sensing images are more effective as they capture microscopic neighborhood features. Meanwhile, the multi-scale remote sensing image representation outperforms those with a single granularity, as it integrates information from remote sensing images of various granularities.